THE JOURNAL OF PHYSICAL CHEMISTRY B

Article

pubs.acs.org/JPCB

Oxidative Destruction of Multilayer Diisopropyl Methylphosphonate Films by O(^{3}P) Atomic Oxygen

Rebecca S. Thompson, Grant G. Langlois, and S. J. Sibener*

The James Franck Institute and Department of Chemistry, The University of Chicago, 929 East 57th Street, Chicago, Illinois 60637, United States

ABSTRACT: We present work detailing the oxidative destruction of the nerve agent simulant diisopropyl methylphosphonate (DIMP) with O(^{3}P) using time-resolved, *in situ* reflection absorption infrared spectroscopy (RAIRS) and X-ray photoelectron spectroscopy (XPS). Thermally annealed DIMP films deposited on Au(111) are observed to react upon exposure to a supersonic beam containing O(^{3}P) with average translational energies of 0.12 eV. The reaction is initiated by a hydrogen abstraction from one of three possible sites on DIMP, and then progresses through various secondary reactions with resultant hydroxyl radicals, carbon-centered DIMP-derived radicals, and nondissociated O_2 in the beam. These reactions are accompanied by uptake of oxygen into the film, leading to new hydrogen bonding with the DIMP phosphoryl group. The generated product also presents greater thermal stability than pristine DIMP, suggesting the formation of a distribution of oligomeric and polymeric products. As reactivity is observed to decrease upon continued O(^{3}P) exposure, this product likely forms a protective layer at the vacuum−film interface, hindering destruction of thicker films. Importantly, the rate of reaction and general reactivity trends are the same between DIMP and the smaller simulant dimethyl methylphosphonate (DMMP). The comparable reaction rates of the two molecules coupled with oxygen's inability to erode thick films all the way down to the substrate have specific implications for the development of oxidation-based decontamination strategies for these and other organophosphates in the solid phase. The findings presented in this paper add significant new fundamental understanding of the oxidative chemistry of such species, knowledge needed in order to develop efficacious nerve agent decontamination strategies as well as the refinement of existing models for the dispersal, adsorption, persistence, and destruction of organophosphates in the environment.

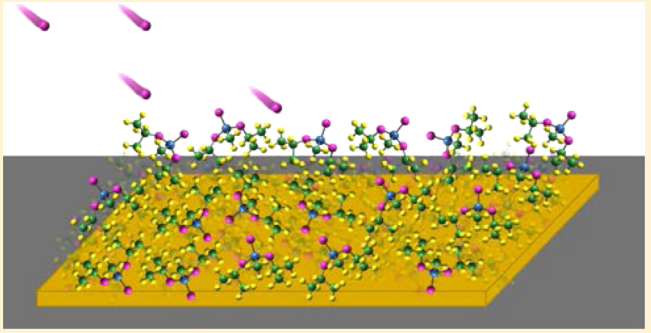

INTRODUCTION

Understanding the oxidative destruction of organophosphates is increasingly essential for national defense and environmental protection.[1,2] Organophosphonate nerve agents like Soman and Sarin remain a significant threat in modern warfare, despite the multinational treaty aimed at preventing their creation and stockpiling.[3] Additionally, less toxic organophosphates are widely used as pesticides and fire-retardant additives.[4,5] Whether combating dangerous exposure to nerve agents, modeling the environmental impact of pest control measures, or exploring the efficacy of flame retardant coatings, it is critical to understand both the atmospheric and condensed phase destruction pathways, persistence, and dispersal of these compounds.[6−9]

In studies of both gas phase and surface adsorbed organophosphate reactivity, it has become clear that oxygen plays a crucial role in the effective destruction of these compounds. Under atmospheric conditions, for example, it is widely accepted that reaction with hydroxyl radicals is the dominant loss process for organophosphates.[8,10−13] The surface-induced, photocatalytic, or thermal destruction of these compounds has also been extensively studied on metals,[14−16] metal oxides,[17−25] and nanoparticle assemblies.[26−29] While metal oxides in particular are often successful in decomposing organophosphates through coordination to surface-bound hydroxyl groups, many are limited by the number of active sites and significantly decreased activity upon repeat cycles of adsorption and reaction. Recently, these limitations were partially alleviated by the addition of ozone to the reaction,[30,31] which again highlights the importance of oxygen in the reliable destruction of these compounds. Even in larger-scale decontamination strategies that involve the use of atmospheric pressure plasma sources,[32−37] the presence of molecular and atomic oxygen species has been shown to improve overall efficacy.[34,37]

In the current study, we present a detailed picture of the oxidative destruction of multilayer diisopropyl methylphosphonate (DIMP) exposed to O(^{3}P). Atomic oxygen in its O(^{3}P) ground electronic state was chosen, as it serves as an aggressive oxidant for simulant destruction while allowing for incisive

Special Issue: Miquel B. Salmeron Festschrift

Received: March 19, 2017
Revised: April 20, 2017

DOI: 10.1021/acs.jpcb.7b02589
J. Phys. Chem. B XXXX, XXX, XXX−XXX

experimental and theoretical mechanistic studies. This work is, in part, an extension of previous research from our lab examining the oxidative destruction of dimethyl methylphosphonate (DMMP).[38] The mechanistic conclusions presented here for the oxidative reactions of both simulants are additionally informed by theoretical investigations of the interaction between organophosphates and reactive oxygen species.[8,39−41] The isopropyl groups in DIMP provide an additional structural similarity with the nerve agent Sarin as well as the possibility of observing alkyl reaction channels unseen in DMMP.[11] Through the use of *in situ* reflection−absorption infrared spectroscopy (RAIRS) and X-ray photoelectron spectroscopy (XPS), we are able to conclusively demonstrate oxidative destruction between adsorbed DIMP and O(^{3}P) under ultrahigh vacuum (UHV) conditions, and compare that to the analogous reaction with DMMP. For both simulants, an oxygen-enriched, thermally stable product is formed upon exposure to O(^{3}P). Additionally, the overall rate of oxidative destruction is identical between the two molecules, despite the differences in functional groups. As such, the findings contained herein have important implications for the solid phase destruction of organophosphates; future decontamination and environmental modeling techniques will have to take into account the fact that the relative rates, byproducts, and persistence of these compounds may vary greatly between the condensed and gaseous phases.

EXPERIMENTAL SECTION

All experiments described in this work were performed in a molecular beam scattering instrument described in detail in a previous publication.[42] A triply differentially pumped molecular beamline exits in a UHV chamber, in which a single-crystal Au(111) sample is exposed to a supersonic atomic oxygen beam and the subsequent interfacial changes are monitored in real time using *in situ* RAIRS and XPS. The substrate, Au(111), was chosen for this study because it is both inert to simulant films and sufficiently reflective for the use of RAIRS.

Most of the experimental details described here are identical to those used in a recent paper on the analogous reaction between O(^{3}P) and DMMP films.[38] One difference, however, is in the method for simulant film deposition. For these experiments, DIMP was dosed on the Au(111) crystal surface through the beam source; 5% O_2 in neon was used as the carrier gas for dosing, and all beamlines were pumped out to remove trace DIMP prior to turning on the O(^{3}P) source for reaction. RAIR spectra were collected with a Nicolet 6700 infrared spectrometer: p-polarized IR radiation is reflected from the Au(111) substrate at a 75° incident angle and collected in a liquid-nitrogen-cooled MCT/A detector. Spectra, averaged over 200 scans at 4 cm^{-1} resolution and fit to Gaussian peaks with linear baselines, were used to quantify DIMP film thickness and characterize products and reaction progress during exposure. A representative spectrum of a 27-layer DIMP film is shown in Figure 1, with the three characteristic regions most frequency referenced herein (P—O—C, P═O, and C—H stretches) highlighted in color. The respective peak assignments are consistent with expectations and values previously reported in the literature.[18,43−46]

Films were prepared by first dosing DIMP onto the substrate at 165 K, under conditions where DIMP desorption is negligible. Immediately following the dosing, films were annealed at 182 K until the desired initial thickness was reached. In order to correlate RAIR signal with a particular DIMP film thickness, isothermal desorption experiments were

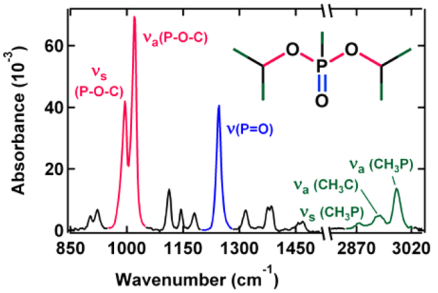

Figure 1. RAIR spectra of a 30-layer-thick DIMP film deposited on single-crystal Au(111). Signals referred to in the text include the P—O—C (pink; 995 and 1020 cm^{-1}), P═O (blue; 1245 cm^{-1}), and C—H (green; 2880, 2931, and 2981 cm^{-1}) stretching modes. All modes are highlighted in the DIMP spectrum and molecule inset.

performed within the range 173−175 K. By tracking the integrated area of the P−O−C signals over time, it was possible to distinguish multilayer from monolayer DIMP. As shown in Figure 2, the rate of desorption changes abruptly upon reaching

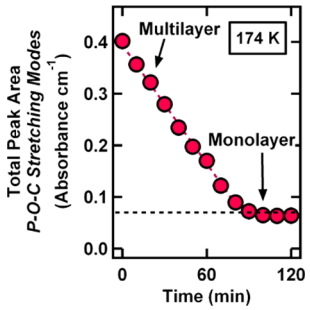

Figure 2. Isothermal desorption of a DIMP film at 174 K showing a clear distinction between multilayer and monolayer desorption rates, as tracked via integration of P−O−C signals. The value at which the rate changes corresponds to the infrared intensity of a single layer of DIMP.

the monolayer, which allows for the quantitative determination that a monolayer of DIMP corresponds to an average total integrated P−O−C intensity of 0.07 absorbance units cm^{-1} using our current setup. This value was used to quantify initial DIMP film thicknesses for all trials; peak line shapes remained consistent beyond 30 layers, the maximum thickness referenced in this study.

Supersonic expansions of atomic oxygen were generated through the use of a radio frequency plasma source described previously.[47] In brief, ignition of a starting gas mixture of 5% O_2 in neon results in expansions containing 35−60% O(^{3}P). We conclude that our beam is virtually devoid of the potentially reactive species O^+ and O(^{1}D) due to the use of a 2000 V/cm deflecting field region and careful selection of low RF power and gas backing pressure. The beam therefore contains primarily O(^{3}P), nondissociated O_2, and neon. O(^{3}P) flux and translational energy are calculated via time-of-flight experiments. The pressure rise in the chamber (as measured with a nude Bayard−Alpert ion gauge), the chamber pumping speed, the relative sensitivity of the gauge to O_2,[48,49] and the spot size on the Au(111) crystal were used to calculate the flux of a neat O_2 beam.[50] Once the fraction of O_2 dissociation was determined for a particular experiment, the integrated peak areas of O_2 time-of-flight spectra obtained with an in-line quadrupole mass spectrometer were used to calculate the total

DOI: 10.1021/acs.jpcb.7b02589
J. Phys. Chem. B XXXX, XXX, XXX−XXX

$O(^3P)$ flux. Typical average translational energies and fluxes of $O(^3P)$ from the beam impinging at normal incidence were, respectively, 0.12 eV and 2×10^{17} atoms cm^{-2} s^{-1}. The average beam energy distribution width was 0.07 eV.

It is important to note that, while the experimental conditions for $O(^3P)$ exposure are the same as our recent study, all of the DIMP reactivity experiments discussed herein involved significantly greater *total* $O(^3P)$ exposures than those in the aforementioned DMMP publication.[38] As such, DMMP experiments were repeated with this increased exposure to better compare the two molecules. This change did not significantly alter any of our previous conclusions; the details of any minor refinements are referenced in the Results and Discussion section.

For XPS experiments, an Al Kα (1486.6 eV) X-ray source (PHI model 04-151) operating at 10 kV and 20 mA irradiated the sample with X-rays at a 45° incident angle. Spectra in the C(1s), O(1s), and Au(4f) regions were collected using a double pass cylindrical mirror analyzer (PHI model 15-255G) with a 50 eV pass energy and 0.4 eV step size. Resultant peaks were fit in the same manner as that used in RAIRS analyses, and the binding energy scale was calibrated in reference to the intense pair of Au(4f) peaks at 87.63 and 83.95 eV.[51]

RESULTS AND DISCUSSION

Spectral Evidence of Reaction. As with DMMP, numerous transformations are observed in the RAIR spectra of a DIMP film exposed to $O(^3P)$. Changes in four important spectral regions are highlighted in Figure 3 for a seven-layer

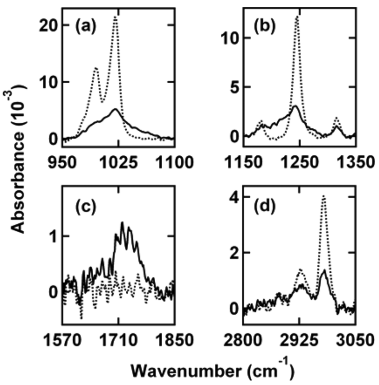

Figure 3. RAIR spectra of characteristic regions of a seven-layer DIMP film before (dashed line) and after exposure to $O(^3P)$ (solid line; total exposure of ~1×10^{21} atoms cm^{-2}). The total signal intensity is observed to decrease in the P—O—C (a), P═O (b), and C—H (d) regions, but new signal growth is also observed in parts a and b. New peaks grow in upon exposure in between 1650 and 1750 cm^{-1} (c). Further explanation of all peak intensity changes and shifts is given in the text.

film. We note here (and discuss further in the Product Formation section) that the observed oxidative reactivity is independent of the original DIMP film thickness for the $O(^3P)$ exposures considered in this study. The original peaks associated with pristine DIMP are clearly observed to decrease in intensity upon exposure. In the P—O—C region (Figure 3a), it is the 995 and 1020 cm^{-1} signals that decay; these peak locations match reported values for the asymmetric and symmetric P—O—C stretches.[18,43−46] This decay corresponds to reactive destruction of these modes.[38] Concurrent with this destruction, however, new intensity is observed between 1030 and 1100 cm^{-1}. The broadness of this new region makes exact peak fitting difficult, but a good fit was routinely established with peaks at 1041 and 1063 cm^{-1}. These peak locations are also nearly identical to our recorded values for adsorbed DMMP,[38] which suggests that they may correspond to the same asymmetric and symmetric P—O—C stretches in a phosphonate ester with smaller alkyl groups. It has been reported that the P—O—CH_3 peak locations are 40−60 cm^{-1} greater than those associated with P—O—iPr.[52] Alternatively, these signals may be due to the formation of new P—O or P—O—H groups. The locations and broadness of these modes are consistent with reported values for various amorphous or glassy phosphate species.[37,53−57]

The P═O region (Figure 3b) undergoes a similar transformation on exposure to $O(^3P)$. The pristine DIMP film has a single peak at 1245 cm^{-1}, which is consistent with reported values for the P═O stretch in gas and liquid phases or adsorbed on unreactive, nonhydroxylated surfaces.[43−46] With $O(^3P)$ exposure, the 1245 cm^{-1} mode decays and is replaced by a new signal at 1216 cm^{-1}. As was reported for DMMP, this red-shifted peak location is the result of the P═O moiety coordinating to surface hydroxyl groups, water, or other hydroxyl-terminated species through hydrogen bonding.[22,44,52,58,59] Therefore, unlike the P—O—C region, the decrease in intensity of the original P═O peak does not correlate with reactive destruction of P═O modes. Rather, the reaction of DIMP with $O(^3P)$ generates hydrogen bonding sites within the film, resulting in some fraction of the DIMP becoming partially solvated by hydrogen bonds. This is supported by Figure 4, which shows the absolute areas lost and gained by peaks in the P═O (Figure 4a) and P—O—C (Figure 4b) regions. Clearly, the loss of area in the 1245 cm^{-1} signal tracks almost exactly with the area gained in 1216 cm^{-1}. This is unlike the behavior of the P—O—C peaks, for which

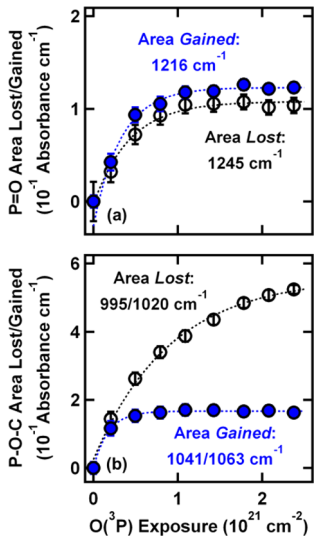

Figure 4. Changes in integrated peak areas are shown for the P═O (a) and P—O—C regions (b) of a 27-layer DIMP film. The area *lost* from peaks associated with pristine DIMP is shown in black (1245 cm^{-1} for P═O and 995 and 1020 cm^{-1} for P—O—C, while the area *gained* by new peaks is shown in blue (1216 cm^{-1} for P═O and 1041 and 1063 for P—O—C). In the P═O region, intensity shifts away from the original peak due to solvation by new hydrogen bonds. Conversely, in the P—O—C region, the original peaks continue to decay in intensity long after the new peaks have stopped growing in.

DOI: 10.1021/acs.jpcb.7b02589
J. Phys. Chem. B XXXX, XXX, XXX−XXX

area growth and loss appear unrelated. Therefore, the P═O region is exhibiting a red shift in the original band.

In the C−H region (Figure 3d), the three original peak locations are consistent with literature values for asymmetric P−CH_3 (2981 cm^{-1}), asymmetric C−CH_3 (2931 cm^{-1}), and symmetric P−CH_3 stretches (2880 cm^{-1}).[18,44,46] All three peaks decrease in intensity during the reaction but no new peaks or shifts are observed, supporting reactive destruction of DIMP. The fact that all three of these modes are observed to decrease in intensity indicates that the system has enough energy to overcome the barriers for reaction at each of the C−H sites visible in the RAIR spectra (P−CH_3 and C−CH_3). The tertiary C−H stretch of the isopropoxy group is unresolved in our spectra, but theoretical barriers for hydrogen abstraction are comparable for both possible sites on the isopropoxy groups, so the reaction is likely occurring at the tertiary site as well.[8,39,40]

The final change observed in the reacted DIMP RAIR spectra yet to be discussed is the growth of a broad pair of peaks at 1645 and 1724 cm^{-1} (Figure 3c). Carbonyl-containing species with similar peak locations have been identified as products or intermediates in a number of prior organophosphate studies, including destructive adsorption on metal oxides,[24,27,60] gas-phase reactions with hydroxyl radicals under atmospheric conditions,[11] and destruction with a radio frequency plasma source.[37] Probable sources of these new C═O bands are addressed in the next section.

Product Formation. Oxidative destruction of both DIMP and DMMP begins with a hydrogen abstraction step leading to formation of a carbon-centered radical. This is supported by a myriad of both theoretical and experimental work concluding that hydrogen abstraction is the most energetically accessible channel for these organophosphates. We cite, for example, recent theoretical gas phase calculations for $O(^3P)$ and Sarin (nerve gas for which DMMP and DIMP are both simulants), which report that the upper limits for hydrogen abstraction barriers are 0.47, 0.20, and 0.19 eV for abstraction from the methyl, isopropoxy tertiary C−H, and CH_3 sites, respectively.[39,40] While some of these projected barriers are larger than the current study's mean beam energies (accounting for the energy distributions), there are a few reasons why hydrogen abstraction is nevertheless feasible. First, the barriers are likely lower in the solid phase due to formation of longer-lived collision complexes in the film. This assertion is reinforced by experimental evidence indicating that reactions between $O(^3P)$ and organic or hydrocarbon-based films proceed largely through such abstraction mechanisms.[61−63] Second, and perhaps more importantly, while the initial abstraction by $O(^3P)$ may be energetically limiting or rate-limiting, once a hydrogen has been abstracted, hydroxyl radicals are produced. These hydroxyl radicals can continue reacting within the film, and the barriers for hydrogen abstraction from DIMP by hydroxyl radicals are significantly lower.[8,64] One theoretical study concluded that abstraction from all three possible sites by hydroxyl radicals is facile under atmospheric conditions, with barriers at or below 2kT for our system.[8] These low-barrier, secondary abstractions help explain why all of the DIMP C−H stretching peaks are observed to decrease concurrently despite the disparity in barriers for direct abstraction by $O(^3P)$.

Spectral changes in the P═O region, as well as XPS analysis, confirm the continued reaction and retention of oxygen-containing species within the film. In the P═O region, the shift in intensity from 1245 to 1216 cm^{-1} is consistent with the analogous shift observed for DMMP and indicates solvation of the P═O moiety by new hydrogen bonds.[38,65,66] Additionally, XPS data in Figure 5 verify that, even when accounting for the loss of gaseous carbon-containing products such as CO and CO_2,[31] comparison of C(1s) and O(1s) signals between pristine and reacted DIMP films shows a substantial increase in the relative N_O/N_C ratio at the surface.

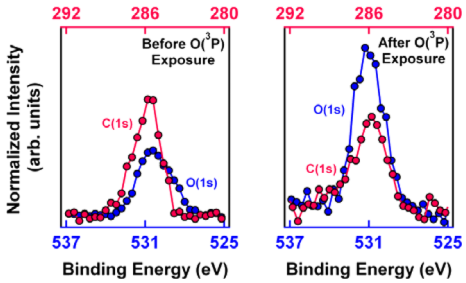

Figure 5. XPS data of 17-layer DIMP films as deposited and after $O(^3P)$ exposure demonstrating that the N_O/N_C ratio increases, confirming oxygen is incorporated into the film. The data are scaled such that the carbon (1s) peak areas are equivalent in both films, which accounts for the fact that some carbon is also lost as gaseous species during reaction.

A number of studies have examined the radical reactions of organophosphates under atmospheric and aqueous conditions, and have proposed relevant pathways that provide a useful mechanistic foundation for this work.[8,10−13,41,67−69] Following the rate-determining hydrogen abstraction by $O(^3P)$ or hydroxyl radical, it is likely that O_2 from the beam adds to the resultant carbon-centered radicals, forming peroxy radicals (RO_2•).[8,70−73] These radicals have a number of possible subsequent reaction pathways, including reactions 1 and 2 detailed in Figure 6.[70,74,75] Reaction 1 presents a clear explanation for the uptake of oxygen in the film that is observed with XPS, since both of the nonradical products have new oxygen-containing functional groups. Additionally, these products account for both the observed increase in hydrogen bonding within the film and the appearance of bands in the C═O stretching region of the RAIR spectra. Reaction 2, on the other hand, is not a termination reaction and therefore presents yet another set of possible reaction pathways, detailed in reactions 3 and 4 in Figure 6.[76−79]

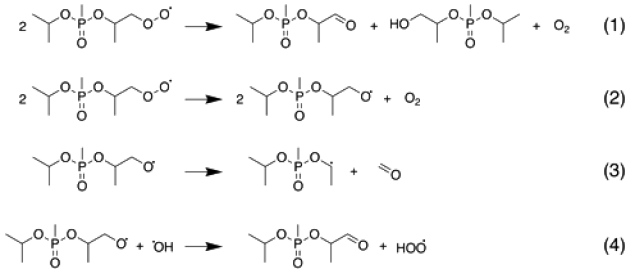

Figure 6. Possible reaction pathways following the hydrogen abstraction from a primary isopropyl carbon in DIMP and subsequent addition of O_2. Reactions include disproportionation (1) to form carbonyl- and hydroxyl-containing products, as well as conversion to alkoxy radical species (2). Alkoxy radicals can undergo unimolecular decomposition (3) or further reaction with hydroxyl radicals in the film (4).

These latter reactions provide further evidence for carbonyl-containing products, as well as a product with a smaller alkoxy

DOI: 10.1021/acs.jpcb.7b02589
J. Phys. Chem. B XXXX, XXX, XXX−XXX

group, possibly accounting for the new bands observed in the P−O−C region of reacted DIMP. Because the initiating hydrogen abstraction step can occur at all three possible sites, there are, of course, a great many more possible reaction pathways than just those discussed here, including combinations and cross-reactions between different radical species. While gas phase barriers, rate constants, and branching ratios have been reported for many of the analogous alkoxy and peroxy radical reactions and decompositions, they are difficult to reliably apply to such a complex solid phase system, whose spectroscopic bands tend only to broaden and convolute. The spectroscopic evidence and mechanisms presented here do, however, largely align with atmospheric studies of DMMP and IMMP (isopropyl methylphosphonate). The products of the reaction between hydroxyl radicals and IMMP, for example, include formaldehyde and acetone as well as the carbonyl-containing phosphonate, $iPrOP(O)(CH_3)OC(O)CH_3$.[11] A distinct P—O—C═O band is unidentifiable in the data presented here, but this mode possibly overlaps with DIMP's P—O—C stretches or may also simply be too small and broad to detect on top of the lower wavenumber DIMP peaks.[52]

Another consequence of the reactions taking place in a solid film is that reaction products and intermediates are in close spatial proximity. Therefore, it can be expected that some of the combination reactions may lead to various cross-linked and higher molecular weight oligomeric and polymeric products (referenced herein as simply "polymeric products"). Polymeric byproducts have been reported during investigations of the decomposition of organophosphates under both gaseous and surface-adsorbed conditions.[33,80] It is often difficult, spectroscopically, to conclusively identify evidence of P−O−P or P−R−P stretching modes, because they either overlap with other absorption bands or appear as smaller, broader peaks.[52] Instead, evidence of a polymeric product is found by monitoring the thermal stability of the film after reaction. After a DIMP film has been exposed to $O(^3P)$, the surface temperature is systematically increased from 165 to 350 K at 0.05 K/s and held constant at a series of intermediate temperatures for the duration of a spectrum acquisition. For comparison, a pristine film is subjected to identical treatment. A representative summary of this data for the P−O−C region is given in Figure 7. Clearly, the thermal stability of a reacted DIMP film is much greater than that of a pristine film. As the RAIR spectra inset shows, unreacted DIMP is fully desorbed by 200 K, whereas a reacted film retains appreciable intensity at 350 K and beyond. Moreover, when the reacted film does begin to desorb, intensity is lost from the original P−O−C peaks first, indicating that unreacted DIMP is eventually freed. This increase in product stability cannot be explained fully with the initial unimolecular and bimolecular reactions given in Figure 6. Rather, radical intermediates likely react in a series of steps, forming the observed oxygen-containing species of higher molecular weight.

As observed in Figure 7, the full retention of spectral intensity for an additional 30 K in a reacted film suggests that even the *unreacted* DIMP possesses some increased thermal stability on the substrate following $O(^3P)$ exposure. A possible explanation for this is that the oxidative reaction begins at the vacuum−film interface and progresses layer by layer into the film. The subsequent reactions lead to the formation of a thermally stable, polymeric overlayer on top of the remaining unreacted DIMP. Until the surface temperature is high enough to destroy or increase the mobility of this polymeric overlayer, the unreacted DIMP is effectively trapped on the surface.

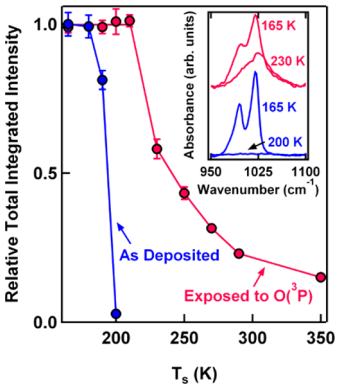

Figure 7. Stepped isothermal desorption experiments on pristine (blue) and reacted (pink) 17-layer films show that DIMP exposed to $O(^3P)$ exhibits much greater thermal stability on the substrate. In the reacted film, the integrated intensity of the P−O−C region (normalized to the original film thickness) begins to decrease at a surface temperature approximately 30 K higher than the point at which the pristine film decreases. RAIR spectra in the corresponding region of each of the simulants are displayed in the inset.

Evidence for this type of "top-down" reactivity is presented in Figure 8, which shows the absolute area lost from the original

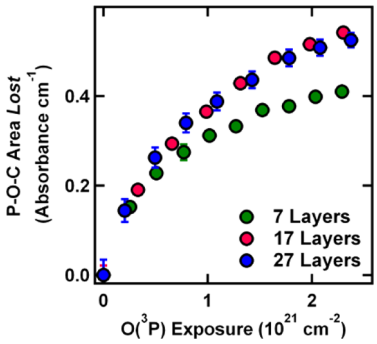

Figure 8. RAIR spectra for 7-, 17-, and 27-layer DIMP films showing that reaction probability decreases with continued $O(^3P)$ exposure. The data shown are the integrated areas *lost* from the original P−O−C peaks (995 and 1020 cm^{-1}) upon $O(^3P)$ exposure. The overlap of the data confirms that multilayer reactivity is independent of original film thickness and likely initiates at the vacuum−film interface. The earlier turnover of the seven-layer film likely reflects the reaction front beginning to terminate as it approaches the film−substrate interface.

P−O−C peaks in a 7-, 17-, and 27-layer DIMP film as they are exposed to $O(^3P)$. Regardless of initial film thickness, the reaction progresses at the same rate. The reaction then begins to slow as either the film is completely eroded or, in the case of thicker films, the $O(^3P)$ is simply unable to penetrate and continue reacting in the bulk. This decay, like for DMMP, therefore does not follow simple first- or half-order kinetics with respect to $O(^3P)$ exposure. *The formation of the polymeric overlayer thus hinders not only desorption of unreacted DIMP but also the destruction of thicker films all the way down to the substrate*. This experiment was repeated with DMMP under the same heating rate conditions for exact comparison. The same trends emerge: a stark increase in thermal stability of the reacted product, and when desorption begins, it is the unreacted simulant that desorbs first.

Comparison of DIMP and DMMP Reactivity. Qualitatively, there are many similarities in the behavior of DIMP

DOI: 10.1021/acs.jpcb.7b02589
J. Phys. Chem. B XXXX, XXX, XXX−XXX

and DMMP films exposed to $O(^3P)$. In Figure 9, the RAIR spectra of both reacted films show the following: a decrease in

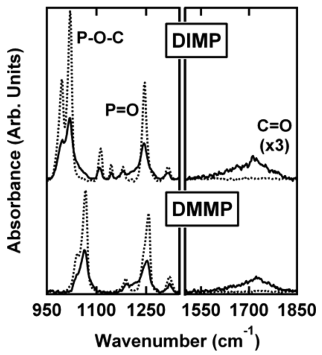

Figure 9. Analogous changes are observed in the RAIR spectra of pristine (dashed) and reacted (solid) 17-layer DIMP and 12-layer DMMP films. C−H modes are not included here due to their low intensity in DMMP spectra.

intensity of the asymmetric and symmetric P—O—C stretches, a red shift of intensity in the P═O stretch, and a broad growth between 1650 and 1750 cm^{-1} that we attribute to new C═O stretching modes. The only key difference is the growth of two new, bluer peaks at 1041 and 1063 cm^{-1} in the P—O—C region of DIMP. These peaks are attributed to products or intermediates in the oxidative destruction of DIMP and are unobserved in DMMP. As such, total reactivity of the two molecules is compared exclusively via decay of the original P—O—C peaks. Such a comparison is shown in Figure 10. Once the P—O—C peak decay is scaled to the integrated intensity of the monolayer (Figure 2), the reactivities of DIMP and DMMP are clearly identical.

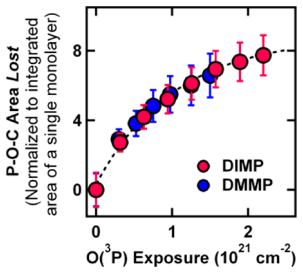

Figure 10. Integrated area lost from the two original P−O−C peaks of both molecules (995 and 1020 cm^{-1} for DIMP, 1041 and 1066 cm^{-1} for DMMP), scaled to respective monolayer areas. The scaled reaction rates for the two simulants are indistinguishable.

Many of the reaction channels presented here for DIMP are possible for DMMP as well. Differences may, however, be expected in the overall reaction rates for the two molecules, due in part to differences in both initial hydrogen abstraction rates and preference for tertiary hydrogen abstraction in the gas phase.[11,70,73] However, the barriers for all possible hydrogen abstractions in DIMP *and* DMMP are comparable in magnitude, especially when considering abstractions by generated hydroxyl radicals.[8,39,40,64] The replicable decay observed in the C−H peaks of both molecules upon $O(^3P)$ exposure attests to the fact that these barriers are indeed accessible by the system. Furthermore, once radicals have begun forming, the close spatial proximity of radical species in the film will likely contribute to a high rate of secondary reactions.[81,82] The multitude of channels available, as well as the accessibility of initial abstractions, leads to the comparable observed overall rates of reaction for DIMP and DMMP in this study.

CONCLUSIONS

The oxidative destruction of solid multilayer DIMP by $O(^3P)$ has been characterized using time-resolved RAIRS and XPS. The reaction begins with hydrogen abstraction from one of three possible sites on the DIMP molecule by an incident $O(^3P)$ or hydroxyl radical intermediate. The resultant carbon-centered radicals go on to either unimolecularly decompose or further react with nondissociated O_2 in the beam or a neighboring radical in the film. The overall destruction per unit dose decays upon continued $O(^3P)$ exposure, independent of film thickness. The products formed during reaction possess greater thermal stability on the substrate than unreacted DIMP, which leads to the conclusion that, at 165 K, 0.12 eV $O(^3P)$ erodes the top layers of a DIMP film, forming an oxygen-containing product overlayer that hinders the continued reaction of DIMP fully down to the substrate. Interestingly, the reactions of $O(^3P)$ and both DIMP and DMMP progress at the same overall rate and lead to similarly persistent polymeric products. This is in contrast to gas phase analyses that find faster rates of oxidation for DIMP.

These findings aid our understanding of condensed phase organophosphate destruction. For example, protection of unreacted compounds afforded by a polymeric overlayer could explain why organophosphates coating inert particles in the atmosphere have longer lifetimes than their gas phase counterparts.[13] Additionally, the clear importance of organophosphate reactions with hydroxyl radicals observed here serves to reinforce our understanding of these compounds' known flame retarding properties.[83]

Extension of this work could examine the oxidative destruction of these compounds on a variety of representative environmental surfaces, both reactive and inert; reactive surfaces may include metal oxides like silica or titania, while inert surfaces may include some organic thin films, water ice, or biopolymers. This will aid in developing nerve agent decontamination strategies and refining existing models for the dispersal, persistence, and destruction of organophosphates in the environment.

AUTHOR INFORMATION

Corresponding Author

*E-mail: s-sibener@uchicago.edu.

ORCID

S. J. Sibener: 0000-0002-5298-5484

Notes

The authors declare no competing financial interest.

ACKNOWLEDGMENTS

This work was sponsored by the Defense Threat Reduction Agency (DTRA) under Grants HDTRA1-11-1-0001 and HDTRA1-16-1-0024. Additional infrastructure support was provided by the NSF-Materials Research Science and Engineering Center at The University of Chicago, Grant No. NSF-DMR-14-20709. Insightful discussions with K. D. Gibson are gratefully acknowledged.

DOI: 10.1021/acs.jpcb.7b02589
J. Phys. Chem. B XXXX, XXX, XXX−XXX

REFERENCES

(1) Ganesan, K.; Raza, S. K.; Vijayaraghavan, R. Chemical Warfare Agents. *J. Pharm. BioAllied Sci.* **2010**, *2*, 166−178.

(2) Jang, Y. J.; Kim, K.; Tsay, O. G.; Atwood, D. A.; Churchill, D. G. Destruction and Detection of Chemical Warfare Agents. *Chem. Rev.* **2015**, *115*, PR1−PR76.

(3) Bothe, M. A. In *The New Chemical Weapons Convention: Implementation and Prospects*; Bothe, M., Ronzitti, N., Rosas, A., Eds.; Kluwer Law International: Cambridge, MA, 1999; pp 1−17.

(4) Smith, C. S.; Metcalfe, E. A Study of Fire-Retardant Mechanisms in the Gas Phase by FTIR Spectroscopy. *Polym. Int.* **2000**, *49*, 1169−1176.

(5) Szinicz, L. History of Chemical and Biological Warfare Agents. *Toxicology* **2005**, *214*, 167−181.

(6) Bartelt-Hunt, S. L.; Knappe, D. R. U.; Barlaz, M. A. A Review of Chemical Warfare Agent Simulants for the Study of Environmental Behavior. *Crit. Rev. Environ. Sci. Technol.* **2008**, *38*, 112−136.

(7) Munro, N. B.; Talmage, S. S.; Griffin, G. D.; Waters, L. C.; Watson, A. P.; King, J. F.; Hauschild, V. The Sources, Fate, and Toxicity of Chemical Warfare Agent Degradation Products. *Environ. Health Perspect.* **1999**, *107*, 933−974.

(8) Hu, S. X.; Yu, J. G.; Zeng, E. Y. Atmospheric Degradation Mechanisms of a Simulant Organophosphorus Pesticide Isopropyl Methyl Methylphosphonate: A Theoretical Consideration. *Int. J. Quantum Chem.* **2013**, *113*, 1128−1136.

(9) Korobeinichev, O. P.; Shvartsberg, V. M.; Shmakov, A. G.; Bolshova, T. A.; Jayaweera, T. M.; Melius, C. F.; Pitz, W. J.; Westbrook, C. K.; Curran, H. Flame Inhibition by Phosphorus-Containing Compounds in Lean and Rich Propane Flames. *Proc. Combust. Inst.* **2005**, *30*, 2353−2360.

(10) Aschmann, S. M.; Tuazon, E. C.; Atkinson, R. Atmospheric Chemistry of Diethyl Methylphosphonate, Diethyl Ethylphosphonate, and Triethyl Phosphate. *J. Phys. Chem. A* **2005**, *109*, 2282−2291.

(11) Aschmann, S. M.; Tuazon, E. C.; Long, W. D.; Atkinson, R. Atmospheric Chemistry of Isopropyl Methyl Methylphosphonate and Dimethyl N,N-Dimethylphosphoroamidate. *J. Phys. Chem. A* **2010**, *114*, 3523−3532.

(12) Martin, P.; Tuazon, E. C.; Atkinson, R.; Maughan, A. D. Atmospheric Gas-Phase Reactions of Selected Phosphorus-Containing Compounds. *J. Phys. Chem. A* **2002**, *106*, 1542−1550.

(13) Liu, Y.; Liggio, J.; Harner, T.; Jantunen, L.; Shoeib, M.; Li, S. M. Heterogeneous OH Initiated Oxidation: A Possible Explanation for the Persistence of Organophosphate Flame Retardants in Air. *Environ. Sci. Technol.* **2014**, *48*, 1041−1048.

(14) Davies, P. R.; Newton, N. G. The Chemisorption of Organophosphorus Compounds at an Al(111) Surface. *Appl. Surf. Sci.* **2001**, *181*, 296−306.

(15) Henderson, M. A.; White, J. M. Adsorption and Decomposition of Dimethyl Methylphosphonate on Platinum(111). *J. Am. Chem. Soc.* **1988**, *110*, 6939−1947.

(16) Smentkowski, V. S.; Hagans, P.; Yates, J. T. Study of the Catalytic Destruction of Dimethyl Methylphosphonate: Oxidation over Mo(110). *J. Phys. Chem.* **1988**, *92*, 6351−6357.

(17) Chen, D. A.; Ratliff, J. S.; Hu, X.; Gordon, W. O.; Senanayake, S. D.; Mullins, D. R. Dimethyl Methylphosphonate Decomposition on Fully Oxidized and Partially Reduced Ceria Thin Films. *Surf. Sci.* **2010**, *604*, 574−587.

(18) Wilmsmeyer, A. R.; Gordon, W. O.; Davis, E. D.; Troya, D.; Mantooth, B. A.; Lalain, T. A.; Morris, J. R. Infrared Spectra and Binding Energies of Chemical Warfare Nerve Agent Simulants on the Surface of Amorphous Silica. *J. Phys. Chem. C* **2013**, *117*, 15685−15697.

(19) Davis, E. D.; Gordon, W. O.; Wilmsmeyer, A. R.; Troya, D.; Morris, J. R. Chemical Warfare Agent Surface Adsorption: Hydrogen Bonding of Sarin and Soman to Amorphous Silica. *J. Phys. Chem. Lett.* **2014**, *5*, 1393−1399.

(20) Wilmsmeyer, A. R.; Uzarski, J.; Barrie, P. J.; Morris, J. R. Interactions and Binding Energies of Dimethyl Methylphosphonate and Dimethyl Chlorophosphate with Amorphous Silica. *Langmuir* **2012**, *28*, 10962−10967.

(21) Kim, C.; Lad, R.; Tripp, C. Interaction of Organophosphorous Compounds with TiO_2 and WO_3 Surfaces Probed by Vibrational Spectroscopy. *Sens. Actuators, B* **2001**, *76*, 442−448.

(22) Mitchell, M. B.; Sheinker, V. N.; Mintz, E. A. Adsorption and Decomposition of Dimethyl Methylphosphonate on Metal Oxides. *J. Phys. Chem. B* **1997**, *101*, 11192−11203.

(23) Panayotov, D. A.; Morris, J. R. Uptake of a Chemical Warfare Agent Simulant (DMMP) on TiO_2: Reactive Adsorption and Active Site Poisoning. *Langmuir* **2009**, *25*, 3652−3658.

(24) Panayotov, D. A.; Morris, J. R. Thermal Decomposition of a Chemical Warfare Agent Simulant (DMMP) on TiO_2: Adsorbate Reactions with Lattice Oxygen as Studied by Infrared Spectroscopy. *J. Phys. Chem. C* **2009**, *113*, 15684−15691.

(25) Segal, S. R.; Cao, L.; Suib, S. L.; Tang, X.; Satyapal, S. Thermal Decomposition of Dimethyl Methylphosphonate over Manganese Oxide Catalysts. *J. Catal.* **2001**, *198*, 66−76.

(26) Gordon, W. O.; Tissue, B. M.; Morris, J. R. Adsorption and Decomposition of Dimethyl Methylphosphonate on Y_2O_3 Nanoparticles. *J. Phys. Chem. C* **2007**, *111*, 3233−3240.

(27) Panayotov, D. A.; Morris, J. R. Catalytic Degradation of a Chemical Warfare Agent Simulant: Reaction Mechanisms on TiO_2-Supported Au Nanoparticles. *J. Phys. Chem. C* **2008**, *112*, 7496−7502.

(28) Mattsson, A.; Lejon, C.; Štengl, V.; Bakardjieva, S.; Opluštil, F.; Andersson, P. O.; Österlund, L. Photodegradation of DMMP and CEES on Zirconium Doped Titania Nanoparticles. *Appl. Catal., B* **2009**, *92*, 401−410.

(29) Li, Y.; Klabunde, K. J. Nanoscale Metal Oxide Particles as Chemical Reagents. Destructive Adsorption of a Chemical Agent Simulant, Dimethyl Methylphosphonate, on Heat-Treated Magnesium Oxide. *Langmuir* **1991**, *7*, 1388−1393.

(30) Mitchell, M. B.; Sheinker, V. N.; Cox, W. W., Jr. Room Temperature Reaction of Ozone and Dimethyl Methylphosphonate (DMMP) on Alumina-Supported Iron Oxide. *J. Phys. Chem. C* **2007**, *111*, 9417−9426.

(31) Mitchell, M. B.; Sheinker, V. N.; Cox, W. W., Jr.; Hardcastle, K. Sustained Room Temperature Decomposition of Dimethyl Methylphosphonate (DMMP) by O_3 on Alumina-Supported MnO_x. *J. Phys. Chem. C* **2011**, *115*, 11514−11524.

(32) Li, Z.; Li, Y.; Cao, P.; Zhao, H. Surface Decontamination of Chemical Agent Surrogates Using an Atmospheric Pressure Air Flow Plasma Jet. *Plasma Sci. Technol.* **2013**, *15*, 696−701.

(33) Moeller, T. M.; Alexander, M. L.; Engelhard, M. H.; Gaspar, D. J.; Luna, M. L.; Irving, P. M. Surface Decontamination of Simulated Chemical Warfare Agents Using a Nonequilibrium Plasma with Off-Gas Monitoring. *IEEE Trans. Plasma Sci.* **2002**, *30*, 1454−1459.

(34) Kim, D. B.; Gweon, B.; Moon, S. Y.; Choe, W. Decontamination of the Chemical Warfare Agent Simulant Dimethyl Methylphosphonate by Means of Large-Area Low-Temperature Atmospheric Pressure Plasma. *Curr. Appl. Phys.* **2009**, *9*, 1093−1096.

(35) Zhu, W.-C.; Wang, B.-R.; Xi, H.-L.; Pu, Y.-K. Decontamination of VX Surrogate Malathion by Atmospheric Pressure Radio-Frequency Plasma Jet. *Plasma Chem. Plasma Process.* **2010**, *30*, 381−389.

(36) Herrmann, H. W.; Henins, I.; Park, J.; Selwyn, G. S. Decontamination of Chemical and Biological Warfare (CBW) Agents Using an Atmospheric Pressure Plasma Jet (APPJ). *Phys. Plasmas* **1999**, *6*, 2284−2289.

(37) Kim, S. H.; Kim, J. H.; Kang, B. K. Decomposition Reaction of Organophosphorus Nerve Agents on Solid Surfaces with Atmospheric Radio Frequency Plasma Generated Gaseous Species. *Langmuir* **2007**, *23*, 8074−8078.

(38) Langlois, G. G.; Thompson, R. S.; Li, W.; Sibener, S. J. Oxidation, Destruction, and Persistence of Multilayer Dimethyl Methylphosphonate Films during Exposure to $O(^3P)$ Atomic Oxygen. *J. Phys. Chem. C* **2016**, *120*, 16863−16870.

(39) Conforti, P. F.; Braunstein, M.; Dodd, J. A. Energetics and Dynamics of the Reactions of $O(^3P)$ with Dimethyl Methylphosphonate and Sarin. *J. Phys. Chem. A* **2009**, *113*, 13752−13761.

DOI: 10.1021/acs.jpcb.7b02589
J. Phys. Chem. B XXXX, XXX, XXX−XXX

(40) Conforti, P. F.; Braunstein, M.; Stearns, J. A.; Dodd, J. A. Collision Dynamics of $O(^3P)$ + DMMP Using a Specific Reaction Parameters Potential Form. *J. Phys. Chem. A* **2012**, *116*, 2506−2518.
(41) Cory, M. G.; Taylor, D. E.; Bunte, S. W.; Runge, K.; Vasey, J. L.; Burns, D. S. Theoretical Methodology for Prediction of Tropospheric Oxidation of Dimethyl Phosphonate and Dimethyl Methylphosphonate. *J. Phys. Chem. A* **2011**, *115*, 1946−1954.
(42) Gibson, K. D.; Killelea, D. R.; Yuan, H.; Becker, J. S.; Sibener, S. J. Determination of the Sticking Coefficient and Scattering Dynamics of Water on Ice Using Molecular Beam Techniques. *J. Chem. Phys.* **2011**, *134*, 034703.
(43) Guilbault, G. G.; Scheide, E.; Das, J. An Experimental Technique for Studying the Infrared Spectrum of Chemisorbed Compounds. *Spectrosc. Lett.* **1968**, *1*, 167−175.
(44) Crooks, R. M.; Yang, H. C.; McEllistrem, L. J.; Thomas, R. C.; Ricco, A. J. Interactions between Self-Assembled Monolayers and an Organophosphonate Detailed Study Using Surface Acoustic Wave-Based Mass Analysis, Polarization Modulation-FTIR Spectroscopy and Ellipsometry. *Faraday Discuss.* **1997**, *107*, 285−305.
(45) Mott, A. J.; Rez, P. Calculated Infrared Spectra of Nerve Agents and Simulants. *Spectrochim. Acta, Part A* **2012**, *91*, 256−260.
(46) Hameka, H. F.; Carrieri, A. H.; Jensen, J. O. Calculations of the Structure and the Vibrational Infrared Frequencies of Some Methylphosphonates. *Phosphorus, Sulfur Silicon Relat. Elem.* **1992**, *66*, 1−11.
(47) Sibener, S. J.; Buss, R. J.; Ng, C. Y.; Yuan, T. L. Development of a Supersonic $O(^3P_J)$, $O(^1D_2)$ Atomic Oxygen Nozzle Beam Source. *Rev. Sci. Instrum.* **1980**, *51*, 167−182.
(48) Itikawa, Y. Cross Sections for Electron Collisions with Nitrogen Molecules. *J. Phys. Chem. Ref. Data* **2006**, *35*, 31.
(49) Itikawa, Y. Cross Sections for Electron Collisions with Oxygen Molecules. *J. Phys. Chem. Ref. Data* **2009**, *38*, 1.
(50) Gibson, K. D.; Langlois, G. G.; Li, W.; Killelea, D. R.; Sibener, S. J. Molecular Interactions with Ice: Molecular Embedding, Adsorption, Detection, and Release. *J. Chem. Phys.* **2014**, *141*, 18C514.
(51) Crist, V. B. Handbooks of Monochromatic XPS Spectra Volume 1 - The Elements and Native Oxides. *Handb. Elem. Native Oxides* **1999**, *1*, 1−43.
(52) Thomas, L. C. *Interpretation of the Infrared Spectra of Organophosphorus Compounds*; Heyden & Son Ltd.: London, 1974.
(53) Weber, M.; de Moraes, I. R.; Motheo, A. J.; Nart, F. C. In Situ Vibrational Spectroscopy Analysis of Adsorbed Phosphate Species on Gold Single Crystal Electrodes. *Colloids Surf., A* **1998**, *134*, 103−111.
(54) Weber, M.; Nart, F. C. On the Adsorption of Ionic Phosphate Species on Au(111)—an In Situ FTIR Study. *Electrochim. Acta* **1996**, *41*, 653−659.
(55) Waghe, A.; Kanan, S. M.; Abu-Yousef, I.; Jensen, B.; Tripp, C. P. Infrared Study of UV-Irradiated Tungsten Trioxide Powders Containing Adsorbed Dimethyl Methyl Phosphonate and Trimethyl Phosphate. *Res. Chem. Intermed.* **2006**, *32*, 613−623.
(56) Connor, P. A.; McQuillan, A. J. Phosphate Adsorption onto TiO_2 from Aqueous Solutions: An In Situ Internal Reflection Infrared Spectroscopic Study. *Langmuir* **1999**, *15*, 2916−2921.
(57) Pleshko, N.; Boskey, A.; Mendelsohn, R. Novel Infrared Spectroscopic Method for the Determination of Crystallinity of Hydroxyapatite Minerals. *Biophys. J.* **1991**, *60*, 786−793.
(58) Bermudez, V. M. Computational Study of Environmental Effects in the Adsorption of DMMP, Sarin, and VX on γ-Al_2O_3: Photolysis and Surface Hydroxylation. *J. Phys. Chem. C* **2009**, *113*, 1917−1930.
(59) Kuiper, A. E. T.; van Bokhoven, J. J. G. M.; Medema, J. The Role of Heterogeneity in the Kinetics of a Surface Reaction. I. Infrared Characterization of the Adsorption Structures of Organophosphonates and Their Decomposition. *J. Catal.* **1976**, *43*, 154−167.
(60) Li, Y. X.; Schlup, J. R.; Klabunde, K. J. Fourier Transform Infrared Photoacoustic Spectroscopy Study of the Adsorption of Organophosphorus Compounds on Heat-Treated Magnesium Oxide. *Langmuir* **1991**, *7*, 1394−1399.
(61) Garton, D. J.; Minton, T. K.; Alagia, M.; Balucani, N.; Casavecchia, P.; Volpi, G. G. Reactive Scattering of Ground-State and Electronically Excited Oxygen Atoms on a Liquid Hydrocarbon Surface. *Faraday Discuss.* **1997**, *108*, 387−399.
(62) Garton, D. J.; Minton, T. K.; Alagia, M.; Balucani, N.; Casavecchia, P.; Gualberto Volpi, G. Comparative Dynamics of $Cl(^2P)$ and $O(^3P)$ Interactions with a Hydrocarbon Surface. *J. Chem. Phys.* **2000**, *112*, 5975−5984.
(63) Paz, Y.; Trakhtenberg, S.; Naaman, R. Reaction between $O(^3P)$ and Organized Organic Thin-Films. *J. Phys. Chem.* **1994**, *98*, 13517−13523.
(64) Burns, D. S.; Cory, M. G.; Taylor, D. E.; Bunte, S. W.; Runge, K.; Vasey, J. L. A Comparison of Primary and Secondary Hydrogen Abstraction from Organophosphates by Hydroxyl Radical. *Int. J. Chem. Kinet.* **2013**, *45*, 187−201.
(65) Eaton, G.; Harris, L.; Patel, K.; Symons, M. C. R. Infrared and Nuclear Magnetic Resonance Spectroscopic Studies on the Solvation of Trimethylphosphate and Dimethylphosphonate. *J. Chem. Soc., Faraday Trans.* **1992**, *88*, 3527−3531.
(66) Bertilsson, L.; Potje-Kamloth, K.; Lieβ, H.-D. Molecular Interaction of DMMP and Water Vapor with Mixed Self-Assembled Monolayers Studied by IR Spectroscopy and SAW Devices. *Thin Solid Films* **1996**, *284−285*, 882−887.
(67) Aschmann, S. M.; Long, W. D.; Atkinson, R. Rate Constants for the Gas-Phase Reactions of OH Radicals with Dimethyl Phosphonate over the Temperature Range of 278−351 K and for a Series of Other Organophosphorus Compounds at ∼ 280 K. *J. Phys. Chem. A* **2008**, *112*, 4793−4799.
(68) Aschmann, S. M.; Long, W. D.; Atkinson, R. Temperature-Dependent Rate Constants for the Gas-Phase Reactions of OH Radicals with 1,3,5-Trimethylbenzene, Triethyl Phosphate, and a Series of Alkylphosphonates. *J. Phys. Chem. A* **2006**, *110*, 7393−7400.
(69) Abbott, A.; Sierakowski, T.; Kiddle, J. J.; Clark, K. K.; Mezyk, S. P. Detailed Investigation of the Radical-Induced Destruction of Chemical Warfare Agent Simulants in Aqueous Solution. *J. Phys. Chem. B* **2010**, *114*, 7681−7685.
(70) Atkinson, R. Gas-Phase Tropospheric Chemistry of Volatile Organic Compounds: 1. Alkanes and Alkenes. *J. Phys. Chem. Ref. Data* **1997**, *26*, 215−290.
(71) Denisov, E. T. Solid-Phase Radical Reactions and Mechanism of Oxidation of Carbon-Chain Polymers. *Russ. Chem. Rev.* **1978**, *47*, 572−586.
(72) Ingold, K. U. Peroxy Radicals. *Acc. Chem. Res.* **1969**, *2*, 1−9.
(73) Aguila, A.; O'shea, K. E.; Tobien, T.; Asmus, K.-D. Reactions of Hydroxyl Radical with Dimethyl Methylphosphonate and Diethyl Methylphosphonate. A Fundamental Mechanistic Study. *J. Phys. Chem. A* **2001**, *105*, 7834−7839.
(74) Atkinson, R.; Baulch, D. L.; Cox, R. A.; Crowley, J. N.; Hampson, R. F.; Hynes, R. G.; Jenkin, M. E.; Rossi, M. J.; Troe, J. Evaluated Kinetic and Photochemical Data for Atmospheric Chemistry: Volume II - Gas Phase Reactions of Organic Species. *Atmos. Chem. Phys.* **2006**, *6*, 3625−4055.
(75) Orlando, J. J.; Tyndall, G. S. Laboratory Studies of Organic Peroxy Radical Chemistry: An Overview with Emphasis on Recent Issues of Atmospheric Significance. *Chem. Soc. Rev.* **2012**, *41*, 6294−6317.
(76) Devolder, P.; Fittschen, C.; Frenzel, A.; Hippler, H.; Poskrebyshev, G.; Striebelb, F.; Viskolczc, B.; Ehrstuhl, L. Complete Falloff Curves for the Unimolecular Decomposition of I-Propoxy Radicals between 330 and 408 K. *Phys. Chem. Chem. Phys.* **1999**, *1*, 675−681.
(77) Peeters, J.; Fantechi, G.; Vereecken, L. A Generalized Structure-Activity Relationship for the Decomposition of (Substituted) Alkoxy Radicals. *J. Atmos. Chem.* **2004**, *48*, 59−80.
(78) Atkinson, R.; Carter, W. P. L. Reactions of Alkoxy Radicals under Atmospheric Conditions: The Relative Importance of Decomposition versus Reaction with O_2. *J. Atmos. Chem.* **1991**, *13*, 195−210.
(79) Ferenac, M. A.; Davis, A. J.; Holloway, A. S.; Dibble, T. S. Isomerization and Decomposition Reactions of Primary Alkoxy

DOI: 10.1021/acs.jpcb.7b02589
J. Phys. Chem. B XXXX, XXX, XXX−XXX

Radicals Derived from Oxygenated Solvents. *J. Phys. Chem. A* **2003**, *107*, 63−72.
(80) Zegers, E. J. P.; Fisher, E. M. Gas-Phase Pyrolysis of Diisopropyl Methylphosphonate. *Combust. Flame* **1998**, *115*, 230−240.
(81) Moad, G.; Solomon, D. H. *The Chemistry of Radical Polymerization*, 2nd ed.; Elsevier: Oxford, 2006.
(82) Carlier, M.; Sochet, L.-R. Detection by E.S.R. of Peroxy Radicals: The Importance of Radical-Radical Reactions in the Slow Oxidation of Butane. *Combust. Flame* **1975**, *25*, 309−312.
(83) Korobeinichev, O. P.; Shvartsberg, V. M.; Shmakov, A. G. The Chemistry of Combustion of Organophosphorus Compounds. *Russ. Chem. Rev.* **2007**, *76*, 1094−1121.

DOI: 10.1021/acs.jpcb.7b02589
J. Phys. Chem. B XXXX, XXX, XXX−XXX